Eur. Phys. J. Appl. Phys. **82**, 30502 (2018)

https://doi.org/10.1051/epjap/2018180093

THE EUROPEAN PHYSICAL JOURNAL APPLIED PHYSICS

Regular Article

A single slot micro-ring structure for simultaneous CO_2 and CH_4 gas sensing★

Weijia Zhang, Xin Zhang*, Xiaowei Zhang, Han Jin, Qinghui Jin, and Jiawen Jian*

Faculty of electrical engineering and computer science, Ningbo University, Ningbo 315211, PR China

Received: 16 March 2018 / Received in final form: 29 June 2018 / Accepted: 30 July 2018

Abstract. In this paper, we proposed a single silicon-on-insulator micro-ring structure for detecting two different gas components in the same time from one output spectrum. By introducing slot structure, the sensitivity and selectivity of sensor are improved. Specifically, two different sensing mechanisms are synthesized in this structure, thus output spectrum is impacted by varying concentrations of CH_4 and CO_2 respectively. The resonant wavelength of micro-ring resonator is the absorption peak of CH_4, the concentration of CH_4 can be measured with the light intensity change. Simultaneously, the combined action of CH_4 and CO_2 can cause the shift of resonant wavelength, and the total concentration of CH_4 and CO_2 gas can be obtained through the shift amount. For enhancing the evanescent field fraction in slot area and tuning the resonant wavelength of micro-ring being located on the absorption peak of CH_4 (around 3.31 μm), the parameters of slot micro-ring structure, including height of slot in silicon, slot width, radius of micro-ring, waveguide width and the gap distance in coupling section, are well tailored, meanwhile, the quality factor Q of micro-ring is considered for ensuring a satisfied accuracy of sensor. A simulation based on the finite difference time domain method is implemented and the analysis results show that the sensitivity of sensor reaches 2308 nm/refractive index unit.

1 Introduction

Excess of methane and carbon dioxide in the mine is the main cause of hazardous consequence that has deprived hundreds of lives every year. Therefore, real-time accurate quantification of methane and carbon dioxide gases has far-reaching significance for coal mine safety. Now electrical sensors such as electrochemical sensors [1] and semiconductor sensors [2] are commonly used for gas sensing in this area because of their mini-size, cheapness and low power consumption. However, the low performance in selectivity, life expectancy, and sparking risk severely hinders the advancement of electrical sensors. Therefore, optical sensors that based on infrared absorption are commonly applied in explosive gas detection such as methane and carbon dioxide [3,4], but the instability and complicated optical system restrict the further improvement of micrometer size on-chip optical sensors.

With the development of semiconductor processing technology, highly integrated photonic chips have attracted researchers' attention because of their attractive features such as immunity to electromagnetic interference, low power consumption, compactness, ability for remote sensing, fast response, and high sensitivity [5,6]. A variety of different photonic devices for realizing multi-function can be integrated into one small silicon-on-insulator (SOI) chip. Among these, micro-ring resonator, as a classical photonic component, has been widely used in communication [7], optical filter [8,9], detectors [10], modulators [11,12], sensing and so on. In sensing aspect, biochemical and gas sensors based on micro-ring resonator have been reported by detecting the shift of resonant wavelength [13–17]. A low loss label free bio-sensor with 1550 nm resonance wavelength has been reported [15] and a slot silicon micro-ring resonator for room temperature detection of gas composition and pressure has also been reported with 490 nm/refractive index unit (RIU) sensitivity [16]. A silicon micro-ring refractometric CO_2 gas sensor with a sensitivity of 6×10^{-9} RIU/ppm and a detection limit of 20 ppm in the 0–500 ppm range has been reported [17]. On the other hand, evanescent field absorption sensing mechanism is also a feasible method for gas sensing [18–20]. For instance, a silicon-on-nitride slot waveguide structure for detecting NH_3 gas through the light intensity change in its absorption wavelength of 3 μm has been proposed [21]. Slot structure on micro-ring wavelength has also been reported for enhancing the reaction between gas phenomenon and evanescent field in 1527.5 nm band [16]. However, few silicon photonic gas sensors are reported being able to measure multiple gas components by single component simultaneously.

In this study, we propose a slot-waveguide-based micro-ring resonator, combining the two sensing mechanisms of resonant wavelength shift and evanescent field absorption for the first time to simultaneously measure the concentration of methane and carbon dioxide gas. To meet the demands of sensing, the entire structure of the micro-ring

★ Supported by National Nature and Science Foundation (61601253, 61704094, 61771267) and sponsored by K.C.Wong Magna Fund in Ningbo University.
* e-mails: zhangxin_nbu@163.com, jianjiawen@nbu.edu.cn

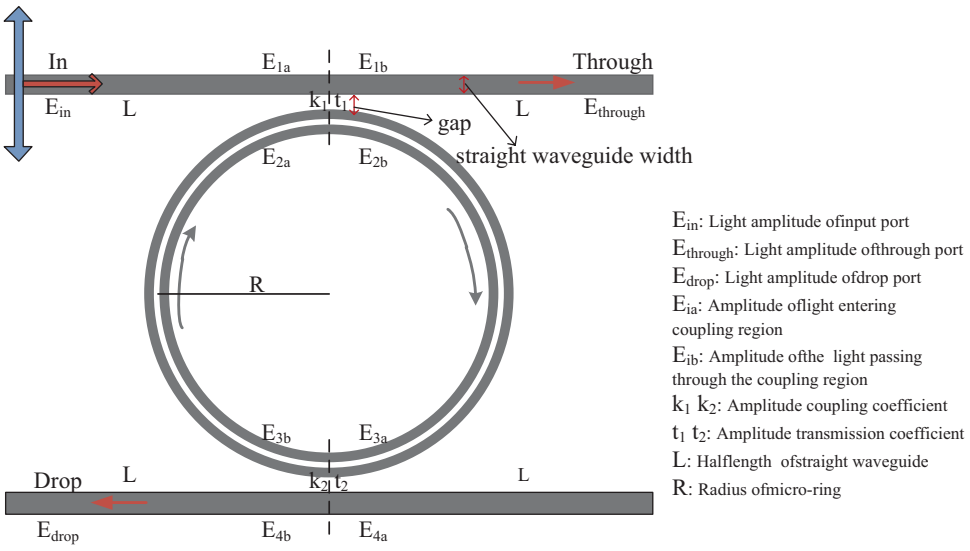

Fig. 1. Structure of designed micro-ring resonator.

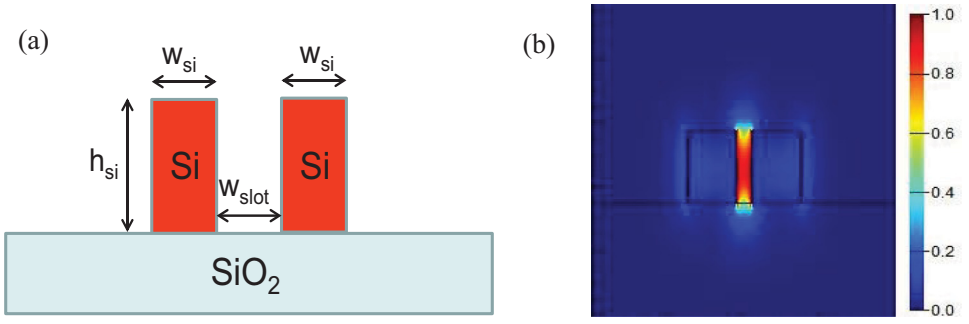

Fig. 2. (a) The cross section of slot ring with three structure parameters slot width(W_{slot}), silicon width(W_{si}) and silicon height(h_{si}). (b) The field distribution of fundamental quasi-TE mode in slot area.

resonator is established and optimized by using finite difference time domain (FDTD) (The core idea of FDTD is to differentiate Maxwell equations in the time and space domain. The specific implementation method is to alternately calculate the electric field and magnetic field in the space domain, and imitate the changes of the electromagnetic field through updating in the time domain). Then the feasibility of measuring methane and carbon dioxide gases by using one micro-ring resonator is numerically analyzed.

2 Structure design

The schematic of core sensing structure is shown in Figure 1, comprising of two straight waveguides and one slot ring. Micro-ring resonator is considered as a promising structure for refractive index sensing because of its high sensitivity and remarkable potential for integrated arrays. Meanwhile, to improve the sensitivity, accuracy and detection limit, slot ring is designed for increasing the interaction between evanescent light field and gas phenomena around the surface of waveguide. The cross section of slot ring is shown in Figure 2a, while the field distribution of quasi-TE mode in the slot area is shown in Figure 2b. According to Figure 2b, it is obvious that the majority of transmission light field is trapped in the slot area, ensuring light intensity be sufficiently absorbed by gas phenomena while resonating in ring slot waveguide. As a result, the slot ring resonator should be tailored so carefully that only 3.31 μm wavelength (absorption peak of CH_4 gas) narrow band light signal is allowed to be resonated in micro-ring.

First, micro-rings with different radius are simulated and the results show that the Q value is consistent with the radius of micro-ring. Taking bending loss into account, we choose the micro-ring radius of 20 μm according to the relationship between bending loss and ring radius in references [22,23]. On the basis of the determined radius, the slot width (W_{slot}), silicon width (W_{si}) and silicon height (h_{si}) of the slot waveguide are optimized for gas absorption by eigenmode expansion solution. Figure 3a, b, and c respectively shows the variation of parameter η which

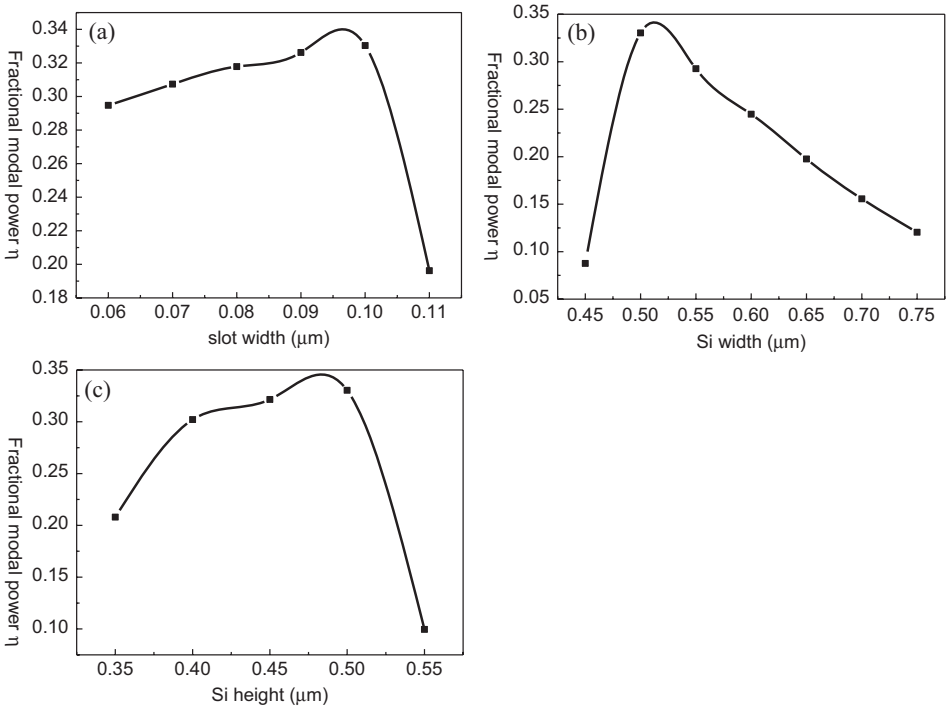

Fig. 3. (a) Variation of η with the different slot width (W_{slot}). (b) Variation of η with the si width (W_{si}) for stable value of W_{slot} and the silicon height (h_{si}). (c) Variation of η with the silicon height (h_{si}) of high index si region.

corresponds to fractional modal power of light trapped in slot area with these three parameters. The parameter η can be expressed as

$$\eta = \frac{\iint_{gas} P_y dxdz}{\iint_{total} P_y dxdz}, \quad (1)$$

where P_y is the y component of the Poynting vector normal to the waveguide cross section. According to the description above, higher value of η represents that more light field is trapped in the low index slot region at the absorption wavelength. The three line charts in Figure 3 show the tendency of η when three parameters increase, namely W_{slot}, W_{si} and h_{si}, respectively.

In Figure 3a, it is obvious that reaches the peak when slot width is 0.1 μm and it decreases rapidly when slot width is beyond 0.1 μm, because the evanescent field is penetrating into the substrate and no longer trapped in the slot area. In contrast, in Figure 3b, as the major fraction of the field enters into the substrate when $W_{si} < 0.5$ μm, the value of η maximized at 0.5 μm. When $W_{si} > 0.5$ μm, the fraction of the field gradually moves to the right high index waveguide with the increase of W_{si}, causing the decrease of η in Figure 3b.

From the curve of Figure 3c, the value of fraction increases with the growing of h_{si}, reaches maximum when h_{si} is 0.5 μm, and then descends significantly. When h_{si} is larger than 0.5 μm, the evanescent field mainly distributes in the high refractive index si waveguide instead of in slot area. Therefore, slot width, silicon width and silicon height are set as 0.1 μm, 0.5 μm and 0.5 μm respectively to trap the biggest proportion of transmission light in slot area. Considering the bend loss of micro-ring resonator, the transmission mode of tailored slot waveguide is shown in Figure 2b, showing that most of light intensity is transmitting in the slot area, ensuring the significance of gas-light interaction.

Despite the dimensions of slot waveguide are determined, other three important parameters in terms of the filter effect, namely the resonator wavelength, extinction ratio and Q factor, are analyzed by modifying straight waveguide width and gap width in coupling section. The simulation result and trend curve of the simulation result are described in Figure 4.

The trend curves clearly show the variation situation of resonant wavelength, extinction ratio, and Q value, and the filter effect of micro-ring resonator influences sensing property significantly in three aspects. First, the resonant wavelength of micro-ring resonator should be exactly located on the absorption peak of CH_4, as it directly impacts the sensitivity of the sensor. Besides, extinction ratio represents the measure range and contrast ratio of the sensor while the Q factor determines the resolution ratio and detection limit. In order to obtain better sensing properties, the structural parameters of the micro-ring resonator are determined: the straight waveguide width is 1 μm and the gap distance is 0.2 μm. In this case, the resonant wavelength of the micro-ring is 3.31503 μm, and by searching the HITRAN database, the absorption coefficient of methane at this wavelength is 33.8 cm^{-1}, the absorption coefficient of carbon dioxide at this wavelength is 0. At the highest point near the red trend curve, the extinction ratio of the resonant wavelength is

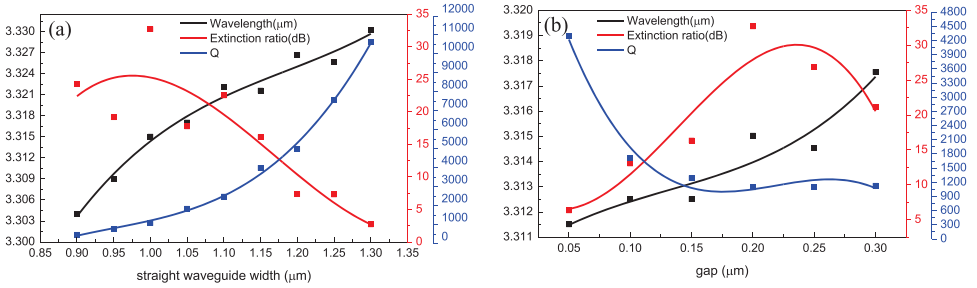

Fig. 4. (a), (b) Simulation result and corresponding trend curves of resonant wavelength, extinction ratio and Q value when the straight waveguide width and gap change respectively.

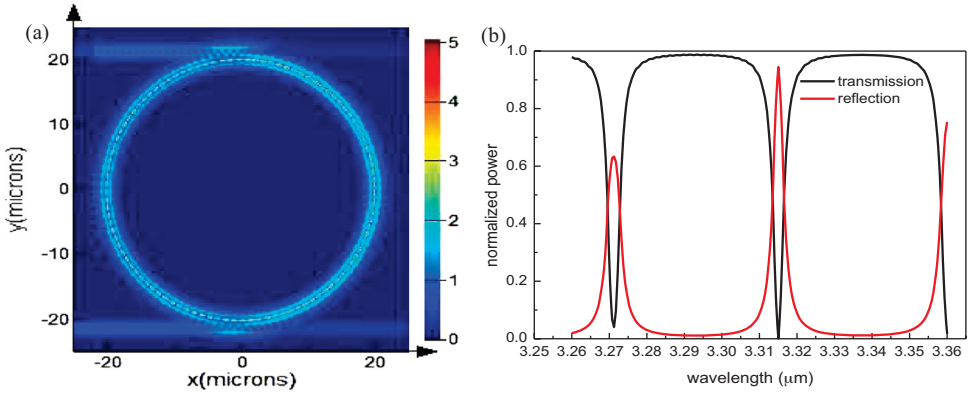

Fig. 5. (a) The optical field distribution diagram. (b) The transmission and reflection output spectrum.

32.70 dB, showing that the micro-ring is close to being critically coupled to the straight waveguide. The Q factor of micro-ring under these parameters is 1093 that basically meets the demand of sensing resolution.

Figure 5a shows the optical field distribution diagram when light signal is transmitting in slot resonator while Figure 5b describes the output spectrum of device.

It can be seen that only the light signal at wavelength of 3.31503 μm resonates well in slot ring. From the output spectrum, the FSR reaches 43.78 nm and the normalized power at resonant wavelength is approaching 0. Therefore, the parameters of slot micro-ring resonator are well tailored for refractive index sensing and intensity absorption sensing.

3 Sensing mechanism and theory calculation

The sensing mechanism includes two parts, one is based on the filter effect in resonant structure and the other is based on the gas absorption during the propagation of the light signal. When input signal is coupled from straight waveguide to slot ring, it follows the resonant equation of

$$2\pi R n_{\mathrm{eff}} = m\lambda, \tag{2}$$

where R is the micro-ring radius, n_{eff} is the effective refractive index of the micro-ring resonator, m represents the resonant order and the value of m is a positive integer, λ is the resonant wavelength. Therefore, only specific wavelength which satisfies the equation can be resonated in the ring and then be coupled into the output straight waveguide as output signal. The transmission matrix of micro-ring resonator can be depicted as,

$$\begin{bmatrix} E_{2a} \\ E_{2b} \end{bmatrix} = \begin{bmatrix} t_1 & -\frac{1}{jk_1} \\ \frac{1}{jk_1} & -\frac{t_1}{jk_1} \end{bmatrix} \begin{bmatrix} E_{1a} \\ E_{1b} \end{bmatrix}, \tag{3}$$

$$\begin{bmatrix} E_{4a} \\ E_{4b} \end{bmatrix} = \begin{bmatrix} t_2 & -\frac{1}{jk_2} \\ \frac{1}{jk_2} & -\frac{t_2}{jk_1} \end{bmatrix} \begin{bmatrix} E_{3a} \\ E_{3b} \end{bmatrix}. \tag{4}$$

Thus, the amplitudes of the output signal in THROUGH port and OUT port are

$$E_{3a} = E_{2b}\exp[-j(\beta - j\alpha_R)\pi R], \tag{5}$$

$$E_{2a} = E_{3b}\exp[-j(\beta - j\alpha_R)\pi R], \tag{6}$$

where k_1, k_2 and t_1, t_2 are respectively the amplitude coupling coefficients and the amplitude transmission coefficients of the upper and lower coupling regions, E_{ia}

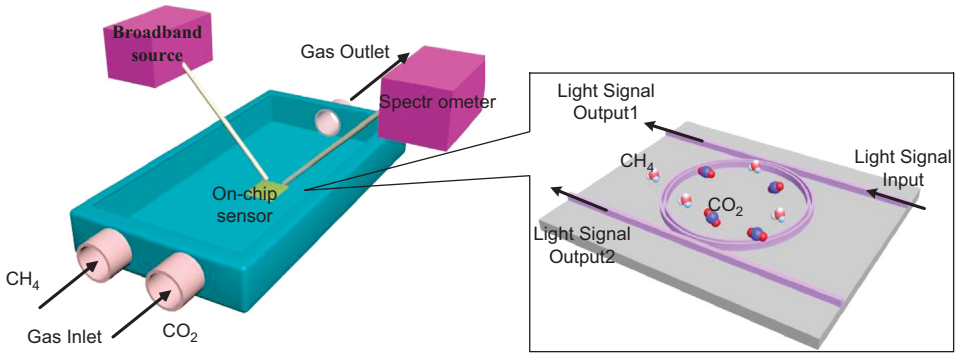

Fig. 6. Diagram of the experimental setup for measuring the transmission spectrum of the device.

is the amplitude of light entering the coupling region, E_{ib} is the amplitude of the light passing through the coupling region, the length of the input and output waveguide is supposed $2L$, $\beta = 2\pi n_{eff}/\lambda$ is the propagation constant which is determined by effective index of waveguide and the wavelength of transmission light. α_L and α_R are transmission losses in straight waveguide and micro-ring waveguide, respectively.

The relationship between wavelength and amplitude of light field can be expressed by transmission matrix and the output spectrum is obtained consequently. The resonant wavelength λ, founded in output spectrum, is determined by micro-ring resonator's effective refractive index n_{eff} that is effectively influenced by external environment. Therefore, an equation expressing the relationship between shift of resonant wavelength and refractive index change of external gas phenomenon can be obtained

$$\Delta\lambda_{resonance} = \frac{\lambda}{n_{eff}}\Delta n_{eff} = \frac{\lambda}{n_{eff}}\Delta n_{gas}\Gamma, \tag{7}$$

where Δn_{eff} is the variation of the effective refractive index, Γ is the interaction factor which satisfies the relationship $\Delta n_{eff} = \Delta n_{eff}\Gamma$. From equation (7), it is obvious that the variety of external refractive index of gas phenomena can be detected by measuring wavelength shift in the output spectrum. Meanwhile, the gas refractive index is related to gas concentration, which can be expressed by the following equation,

$$n' = n \times \frac{x}{100} + n_0 \times \frac{100 - x}{100}, \tag{8}$$

where n_0 represents the pure air refractive index, n represents the refractive index of the target gas, n' is the gas refractive index after mixing, $x\%$ is the target gas concentration. By using this equation, the gas concentration can be obtained if the gas component is known and only one kind of gas is included in the external phenomena. And sensitivity of the sensor S_n is the ratio of the resonance shift to the change of the gas refractive index. The specific mathematical expression is formula (9),

$$S_n = \frac{\Delta\lambda_{resonance}}{\Delta n_{gas}}. \tag{9}$$

However, the target gas always companions with other disturbing gases, being detrimental to accuracy of gas detection. In order to increase the selectivity, another mechanism of gas detection by gas absorption is introduced into this sensing device.

The evanescent wave occurs around the waveguide when the light is transmitted in the waveguide, and specific wavelength of evanescent wave is absorbed by gas phenomenon. As different kinds of gases have different absorption peak, combining with Lambert's law, the gas concentration can be obtained by comparing the light intensity in specific wavelength before and after the gas absorption. The mathematical expression of law can be described by formula (10)

$$I = I_0 e^{-\mu c l}, \tag{10}$$

where I_0 represents the original light intensity, I is the light intensity after gas absorption, μ is the absorption coefficient of the gas at a specific wavelength in cm^{-1}, c is the concentration of the gas in ppm, l is the interaction distance between light and gas. The gas absorption of the specific wavelength can be detected by measuring intensity transmission of the micro-ring resonator sensor. As a result, the selectivity of sensor is ensured by this mechanism when tailored micro-ring resonator allows only sensing wavelength resonate in ring. The sensitivity S_i of the sensor by using this method can be expressed as formula (11)

$$S_i = \frac{\Delta I/I_0}{\Delta c} = \frac{\Delta I_{norm}}{\Delta c}. \tag{11}$$

4 Simulation and discussion

Based on the sensing principle discussed before, the layout of this sensing device is designed as that shown in Figure 6. The gas number of gas inlet and outlet can be self-defined. It can be set multiple for test and only one is needed in real gas component detection. The light source is broadband source and the spectrometer is needed for demodulate light signal. The shift of resonant wavelength can be observed by spectrometer when the gas concentration in gas chamber changes.

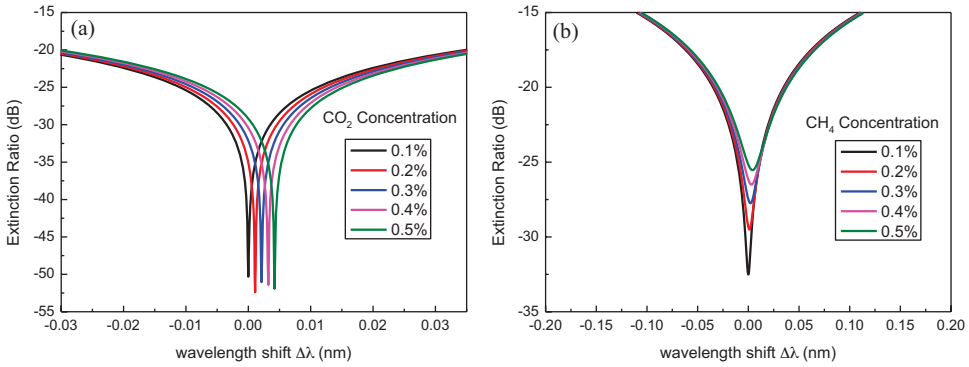

Fig. 7. (a) The wavelength shift $\Delta\lambda$ (respect to 3.2959534 μm) as a function of the concentration of CO_2. (b) The wavelength shift $\Delta\lambda$ (respect to 3.2959534 μm) as a function of the concentration of CH_4.

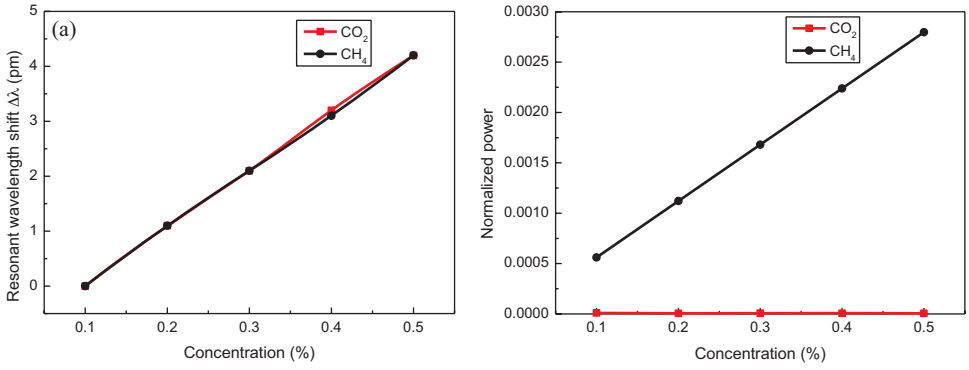

Fig. 8. (a) Relationship of wavelength shift $\Delta\lambda$ (respect to 3.2959534 μm) and gas concentration (0.1–0.5%) when CH_4 and CO_2 exist separately. (b) The value of normalized power (equal to 10^ (Extinction Ratio/10)) at 0.1–0.5% concentration when CH_4 and CO_2 exist separately.

The output spectrum of designed structure is simulated and analyzed by using FDTD solution and transmission matrix method. Two different gas components CH_4 and CO_2, easily found in coal mine circumstance, are measured by designed sensor. As CH_4 and CO_2 have similar refractive index in similar concentration, it is difficult to separate them by detecting wavelength shift. However, if resonant wavelength of micro-ring is located at the sensing wavelength of one of these gases, they can be separated by measuring the output intensity on that wavelength.

Considering the absorption of light, the amplitudes of the output signal of micro-ring in TROUGH port and OUT port can be deduced from formula (5) and (6), which are

$$E_{3a} = E_{2b}\exp[-j(\beta - j\alpha_R)\pi R]\exp[-\mu cl], \quad (12)$$

$$E_{2a} = E_{3b}\exp[-j(\beta - j\alpha_R)\pi R]\exp[-\mu cl], \quad (13)$$

μ is 33.8 cm^{-1}, which is the absorption coefficient of methane at the micro-ring resonant wavelength of 3.31503 μm. $l = \pi R * 10^{-4}$ cm is half of the circumference of the micro-ring resonator. The concentration c range of methane is 0.1–0.5% which represents 1000–5000 ppm.

First, sample gas with single component is added into the gas chamber and the change of output spectrum is observed as shown in Figure 7. Figure 7a describes the spectra when CO_2 gas concentration increases from 0.1% to 0.5% gradually. It is evident that the resonant wavelength of micro-ring experiences a red-shift with the increase of gas concentration. 100 steps in the whole range of CO_2 concentration are simulated and 5 typical concentrations are shown in Figure 7. According to the simulation, the fluctuation of extinction ratio at resonant wavelength is so small that can be ignored compared with depth of resonant notch. Figure 7b describes the spectra in different CH_4 concentrations when the sample gas component only includes CH_4 alone. Unlike CO_2, the extinction ratio of output spectra changes obviously from −33 to −25 dB within the concentration range between 0.1% and 0.5%. At the meantime, the resonant wavelength also red-shifts as concentration grows.

Under certain conditions of simulation accuracy, the specific numerical of resonance wavelength and extinction ratio at different concentration of single gas is shown in Figure 8a and b. Diagram (a) depicts the specific value of resonant wavelength in each concentration point when the CH_4 and CO_2 respectively influence the micro-ring and the resonant wavelength values are the same or very similar in the same concentration of CH_4 and CO_2. The concentration change of CO_2 gas has minimal impact on the extinction ratio at the resonant wavelength, and the concentration change of CH_4 gas regularly affects the change of the extinction ratio from (b).

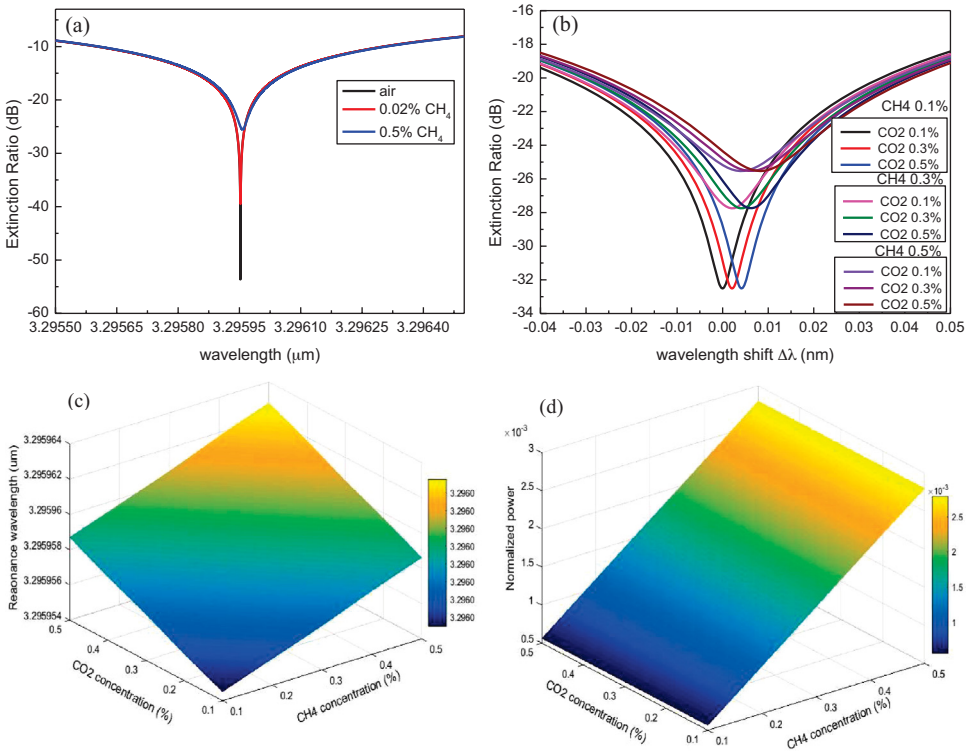

Fig. 9. (a) The output spectra in air, 0.02%CH_4 and 0.5%CH_4. (b) The wavelength shift $\Delta\lambda$ (respect to 3.29545 μm) when CH_4 and CO_2 in different concentrations. (c) Variation of resonant wavelength in mixed gas space with the concentration of CH_4, CO_2 varies from 0.1% to 0.5%. (d) Variation of normalized power (equal to 10^ (Extinction Ratio/10)) at resonant wavelength in mixed gas space.

According to the application circumstance of the sensor, the sample gases mixed by different concentration of two different target gases are detected by the sensor and the spectra of simulation outcome are shown in Figure 9. The output spectra in air, 0.02%CH_4 and 0.5%CH_4 are shown in Figure 9a, the difference of the extinction ratio in air and CH_4 can be easily detected. From Figure 9b, 9 cases of spectra are simulated which describe the spectra in the mixed gas containing both concentration of CO_2 and CH_4 varying in the range from 0.1% to 0.5%. According to Figure 9b, we can conclude that spectra are divided into three stages by different CH_4 concentration. At each stage, the red-shift of resonant peak is influenced by CO_2 concentration. Therefore, the CH_4 concentration can be obtained by measuring the depth of resonant peak and the CO_2 concentration can be obtained from the shift of resonant wavelength of micro-ring. On the other hand, focusing on the similar total concentration of mixed sample gas, the resonant wavelength is observed in similar value. For example, comparing the two case of 0.3%CH_4-0.1% CO_2 and 0.1%CH_4-0.3%CO_2, the resonant wavelength is in similar value around 3.2959565 μm. Therefore, we assume that the depth of resonant peak is only sensitive to CH_4 concentration and the resonant wavelength of slot micro-ring is directly influenced by total concentration of mixed gas. This is because the resonant wavelength of micro-ring is also the peak wavelength in CH_4 absorption spectrum while CO_2 gas has little absorption in this resonant wavelength. Therefore, the two 3D diagrams in (c) and (d) describe the trend of resonant wavelength and normalized power of resonant notch with the increase of two different gas components.

Combined with the above analysis, the mixed gas of CO_2 and CH_4 can be similarly considered as one component of gas in same refractive index since either the single gas or the gas mixture has very little difference in the resonance wavelength shift. So the concentration of methane gas can be obtained by measuring the change of normalized power at the resonant wavelength while the concentration of the mixture gas can be determined by comparing the shift to a set of pre-calibrated reference data by measuring the resonant wavelength. Then the concentration of CO_2 can be obtained by subtracting the concentration of CH_4 calculated by the gas absorption from the total concentration of the mixed gas.

Sensitivity curves of the sensor are shown in Figure 10, the S_n of the sensor is the slope of the curve in Figure 10a with the expression formula (9) and identically the S_i is the slope of the curve in Figure 10b with the formula (11). The specific value of S_n is 2308 nm/RIU in mixed gas and the value of S_i is 5.59×10^{-7} in ppm^{-1} with the concentration range of CH_4 from 0.1% to 0.5%.

5 Conclusion

We have proposed a chip-scale single micro-ring resonator of containing the slot ring based on SOI for simultaneous measurement of the two kinds of gases. Its functional sensing principles are based on shift of resonance

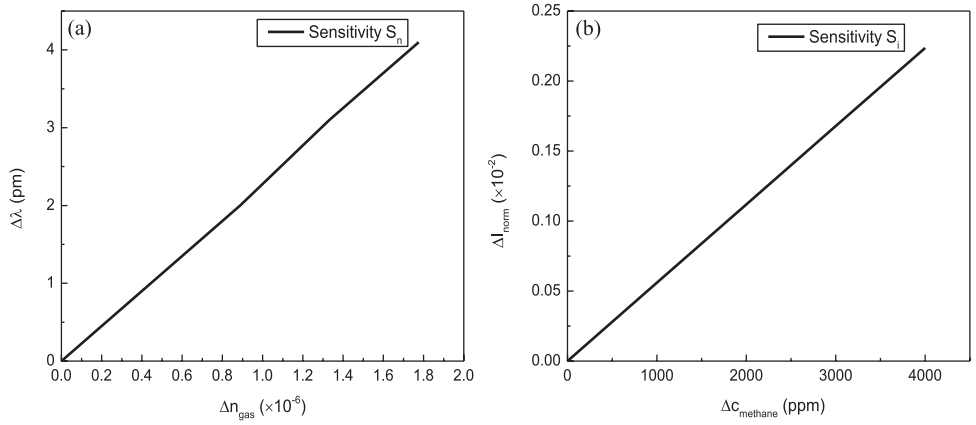

Fig. 10. (a) The relationship between the resonance wavelength shrift and the refractive index difference of the mixed gases. (b) The normalized light intensity at the resonant wavelength varies with the difference in methane concentration.

wavelength and the evanescent field absorption. We have optimized the designed slot waveguide and entire structure of micro-ring resonator to reach the demands of sensing, and the sensing analysis is carried out to demonstrate detectability of CH_4 and CO_2. Based on the two sensing mechanism, the sensitivities of the designed structure are calculated to demonstrate the sensor with the characteristics of good selectivity and high sensitivity. And the research provides a conceptually new strategy for the application of the micro-ring resonator, which has the potential of highly practical for the detection of hazardous gas.

References

1. P.K. Sekhar, J. Kysar, E.L. Brosha, C.R. Kreller, Sens. Actuators B **228**, 162 (2016)
2. B. Mondal, J. Das, C. Roychaudhuri, N. Mukharjee, H. Saha, Eur. Phys. J. Appl. Phys. **73**, 10301 (2016)
3. M. Liu, Z. A. Tang, H. Zhang, Instrum. Tech. Sens. **36**, 18 (2007)
4. J. Hodgkinson, R. Smith, W.O. Ho, J.R. Saffell, R.P. Tatam, Sens. Actuators B **186**, 580 (2013)
5. V.M.N. Passaro, D. Francesco, C. Caterina, M.N. Armenise, Sensors **9**, 1012 (2009)
6. N.A. Yebo, D. Taillaert, J. Roels, D. Lahem, M. Debliquy, Z. Hens, R. Baets, *Symposium of the IEEE Photonics Benelux Chapter* (Optical Society of America (OSA), 2010), p. 141
7. I.S. Amiri, M.R.K. Soltanian, S.E. Alavi, A.R. Othman, M.Z.A. Razak, J. Opt. **45**, 255 (2016)
8. J.Q. Bao, K. Yu, L.J. Wang, J.J. Yin, Opt. Lett. **13**, 268 (2017)
9. Y. Long, J. Wang, Opt. Express **23**, 17739 (2015)
10. M. Hosseinifar, V. Ahmadi, M. Ebnali-Heidari, IEEE Photonics Technol. Lett. **28**, 1363 (2016)
11. J. Hong, F. Qiu, X. Cheng, A.M. Spring, S. Yokoyama, Sci. Rep. **7**, 1 (2017)
12. Q. Xu, S. Manipatruni, B. Schmidt, J. Shakya, M. Lipson, Opt. Express **15**, 430 (2007)
13. C.A. Barrios, K.B. Gylfason, B. Sánchez, A. Griol, H. Sohlström, M. Holgado, R. Casquel, Opt. Lett. **32**, 3080 (2007)
14. A.M. Armani, R.P. Kulkarni, S.E. Fraser, R.C. Flagan, K.J. Vahala, Science (New York, N.Y.) **317**, 783 (2007)
15. M.M. Uzzal, Int. J. Basic Appl. Sci. **14**, 44 (2014)
16. J.T. Robinson, L. Chen, M. Lipson, Opt. Express **16**, 4296 (2008)
17. G. Mi, C. Horvath, M. Aktary, V. Van, Opt. Express **24**, 1773 (2016)
18. M.A. Butt, S.A. Degtyarev, S.N. Khonina, N.L. Kazanskiy, J. Mod. Opt. **64**, 1892 (2017)
19. M.A. Butt, S.N. Khonina, N.L. Kazanskiy, J. Mod. Opt. **65**, 174 (2018)
20. Y. Huang, S.K. Kalyoncu, Q. Song, O. Boyraz, Opt. Commun. **313**, 186 (2014)
21. B. Kumari, A. Barh, R.K. Varshney, B.P. Pal, Sens. Actuators B **236**, 759 (2016)
22. W. Zhang, S. Serna, X.L. Roux, L. Vivien, E. Cassan, *IEEE International Conference on Nanotechnology* (IEEE, 2016), p. 140
23. Q. Xu, D. Fattal, R.G. Beausoleil, Opt. Express **16**, 4309 (2008)

Cite this article as: Weijia Zhang, Xin Zhang, Xiaowei Zhang, Han Jin, Qinghui Jin, Jiawen Jian, A single slot micro-ring structure for simultaneous CO_2 and CH_4 gas sensing, Eur. Phys. J. Appl. Phys. **82**, 30502 (2018)